IPTC International Petroleum Technology Conference

IPTC 16645

Multi-Tubular Corrosion Inspection Using a Pulsed Eddy Current Logging Tool

Marvin Rourke - GOWell Petroleum, Yong Li – Xi'an Jiaotong University, Glyn Roberts – Hemisphere Technologies

This paper was prepared for presentation at the International Petroleum Technology Conference held in Beijing, China, 26–28 March 2013.

Abstract

Tubular inspection can be split between direct measurements such as caliper logs or downhole video observation and Electromagnetic (EM) methods that measure properties sensitive to pipe thickness, with wall thinning associated with corrosion and other pipe defects. Various EM methods have been reported over the years often initially for pipeline inspection and then adapted for downhole well monitoring. These methods include Magnetic Flux Leakage (MFL) and Eddy Current (EC) measurements. Early EM methods were single frequency but later developments include multi-frequency. In this paper we report an emerging technique called Pulsed Eddy Current (PEC) which is inherently multi-frequency and in time domain is radially sensitive which enables inspection of multiple tubular thicknesses. Most inspection techniques including some EM methods are only capable of inspecting the inner most tubular or only the total thickness of multiple tubulars. However, a PEC tool can measure separate thicknesses of both inner and a second tubular. This allows quantitative corrosion evaluation of casing without removing the completion tubing.

The paper covers a theoretical review of the PEC technique and development of a fast forward analytical model tied to experimental data acquired with an actual logging instrument. The fast forward model is used to ensure optimum tool design and allows development of an inverse model which realises quantitative evaluation of the corrosion within multiple tubulars from field data.

Introduction

Well integrity monitoring is growing in importance as fields mature, as oil and gas is exploited in evermore hostile and corrosive environments and due to stricter regulatory requirements. Over the lifetime of a typical well monitoring the completion integrity includes running logs such as cement bond evaluation, production flow logs and tubular inspection. Casing and tubing integrity monitoring often consist of a combination of mechanical multi-finger caliper logs, Ultrasonic inspection logs, ElectroMagnetic pipe thickness logs, compaction monitoring and downhole video recordings. These inspection logs can be used to monitor corrosion early and help mitigate serious leaks or well failures. When combined with other logs that can indicate abnormal flow conditions such as temperature logs, noise or leak detection logs and flow behind casing logs these measurements can assist diagnosis of completion problem that could need intervention. Effective well integrity monitoring is important to evaluate corrosion early and help mitigate serious leaks or well failures.

Background to Pulsed Eddy Current

Compared with Magnetic Flux Leakage (MFL) which is a magnetization-based technique and uses a powerful magnetizer (permanent magnet or DC electromagnet) [1-3], PEC employs a time-variant applied magnetic field. The applied field is generated by an induction coil, namely a driver coil supplied with a transient excitation current in the form of a pulsed, rectangular or step waveform. The applied magnetic field (primary magnetic field) induces eddy currents in conductive specimens as the driver coil is deployed close to the specimen. Any anomalies within the specimen cause perturbation of eddy currents. As a result, the eddy-current-induced magnetic field (secondary magnetic field), which opposes the applied magnetic field, changes in terms of the amplitude and phase. Consequently, the variation in magnitude and phase of the net magnetic field (superposition of primary and secondary magnetic fields) can be found via measurement by pickup coils or solid-state

magnetic field sensors/sensor arrays [4, 5]. Through intensive analysis of the measured signals, the anomalies are detected, identified and quantitatively evaluated.

Due to a broad spectrum of frequency harmonics in its excitation, PEC has better probing penetration and efficiency compared to other eddy current techniques such as Eddy Current (EC) and Remote Field Eddy Current (RFEC) which utilize single-frequency excitation [6, 7]. Information such as the defect size, location, and depth can be obtained in one single excitation process, and analyzed by using features extracted in both time and frequency domains of PEC transient signals. So far PEC has been accepted in industries such as Aerospace, Nuclear Power, etc. Typical applications of PEC in industry involve quantitative evaluation of layered structures of airplanes [8], detection and characterization of flaws in tubes of steam generators of nuclear power plants [9]. The advantages of PEC over other Electromagnetic Nondestructive Evaluation (ENDE) techniques make it a promising method for detection and evaluation of corrosion in multilayered pipe casings.

Verification of an Analytical model for PEC

Suppose a PEC probe is concentrically placed within a layered pipe casing to evaluate corrosion. It is assumed that the width of the corrosion (along z direction) is considerably larger than the thickness of the excitation coil (namely T_x). As a result, the corrosion is analogous to the pipe wall-thinning, and can be taken as a layer with the thickness of d_{L-1}-d_{L-2}, and conductivity of σ_{L-1}. The model is shown in Fig. 1. Based on the Extended Truncated Region Eigenfunction Expansion (ETREE) [10, 11], the PEC signals of magnetic field in frequency domain can be written as:

$$\bar{B}(r,z) = \bar{B}^{II}_{coil} + \bar{B}^{II}_{pipe} \tag{1}$$

$$\bar{B}^{II}_{coil}(r,z) = \frac{2\mu_0 NI}{(r_1-r_2)(z_1-z_2)h}\sum_{i=1}^{\infty}\begin{Bmatrix}-\cos(k_i z)K_1(k_i r)\bar{r}_0\\ -\sin(k_i z)K_0(k_i r)\bar{z}_0\end{Bmatrix}\frac{\left[\cos(k_i z_2)-\cos(k_i z_1)\right]\chi_2(k_i r_1, k_i r_2)}{k_i^2} \tag{2}$$

$$\bar{B}^{II}_{pipe}(r,z) = \frac{2\mu_0 NI}{(r_1-r_2)(z_1-z_2)h}\sum_{i=1}^{\infty}\begin{Bmatrix}-\cos(k_i z)I_1(k_i r)\bar{r}_0\\ \sin(k_i z)I_0(k_i r)\bar{z}_0\end{Bmatrix}\frac{\left[\cos(k_i z_2)-\cos(k_i z_1)\right]\chi_2(k_i r_1, k_i r_2)}{k_i^2}\cdot\frac{V_{II}}{U_{II}} \tag{3}$$

where, I and N denote the excitation current and the number of coil windings, respectively. I_n and K_n denote the modified Bessel functions of the first and second kind, respectively. $k_i=i\pi/h$ (i=1, 2, 3…). The conductor reflection coefficient, V_{II}/U_{II} can be computed via SVD-based matrix method [12] or Cheng's matrix approach [13]. The comparison regarding magnetic field signals in frequency domain between ETREE and Finite Element Modeling (FEM) is presented in Fig. 2. It can be seen from Fig. 2 that the results of ETREE have good agreement (relative error less than 1%) with those of FEM, while the computation time is 3s compared with 203s for FEM. It is noted that the transient PEC signals can be readily derived by using Eqs. (1)-(3) in conjunction with Inverse Fourier Transform (IFT).

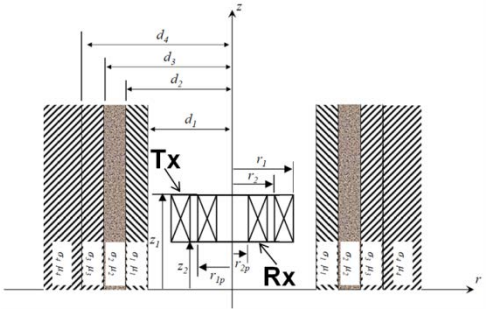

Fig. 1. A 2D axi-symmetric model of PEC of a layered pipe

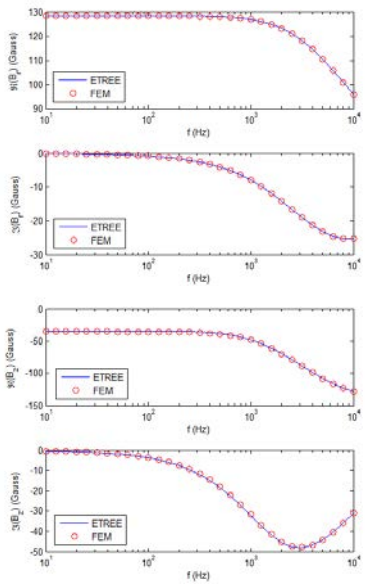

(a) (b)

Fig. 2. Comparison of (a) B_z and (b) B_r between ETREE and FEM

As for the case where a pickup coil (namely R_x, with the number of turns of N', outer and inner radii of r_{1p} and r_{2p} respectively, and height of z_1-z_2) is used to acquire the magnetic field signal, i.e. Electromotive Force (EMF), the EMF signals subject to the excitation coil (V_{coil}) and pipe casings (V_{pipe}) can be individually written as:

$$V_{coil}(t)=\frac{4j\mu_0 N' NI}{(r_1-r_2)(z_1-z_2)^2(r_{1p}-r_{2p})h}\sum_{i=1}^{\infty}\left\{\begin{array}{l}\frac{1}{k_i^6}\left[\cos(k_i z_2)-\cos(k_i z_1)\right]\chi_1(k_i r_1,k_i r_2)\\ \times\left[\cos(k_i z_2')-\cos(k_i z_1')\right]\chi_2(k_i r_1',k_i r_2')\end{array}\right\} \quad (4)$$

$$V_{pipe}(t)=\frac{4j\mu_0 N' N}{(r_1-r_2)(z_1-z_2)^2(r_{1p}-r_{2p})h}\sum_{i=1}^{\infty}\left\{\begin{array}{l}\frac{1}{k_i^6}\left[\cos(k_i z_2)-\cos(k_i z_1)\right]\chi_2(k_i r_1,k_i r_2)\\ \times\left[\cos(k_i z_2')-\cos(k_i z_1')\right]\chi_2(k_i r_1',k_i r_2')\int_{-\infty}^{+\infty}\omega I(\omega)\frac{V_{II}}{U_{II}}e^{j\omega t}d\omega\end{array}\right\} \quad (5)$$

Thus, the predicted EMF signal from R_x is the superposition of V_{coil} and V_{pipe}.

The comparison of transient magnetic field signals and coil EMF signals between ETREE and FEM is presented in Fig. 3. It can be seen from Fig. 3 that ETREE has good agreement with FEM without much loss of accuracy.

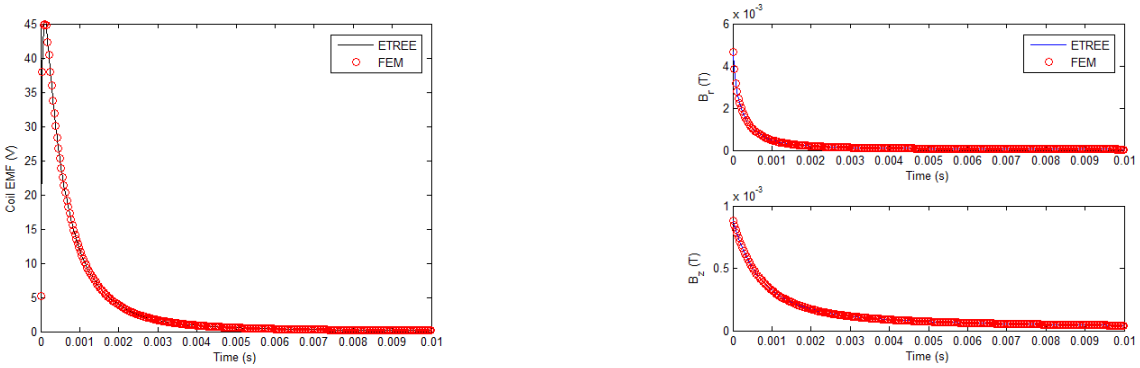

(a) **(b)**

Fig. 3. Comparison of (a) coil EMF signal and (b) magnetic field signals between ETREE and FEM

The coil EMF signals computed via ETREE are also compared with experimental results by using appropriate parameters for the coils, tool housing and pipe casings. In practical measurements the Time-Slice-Integration feature (TSI) is adopted for evaluation of thicknesses of inner and outer pipe casings. As a result, after predicted signals are computed via ETREE, Trapezoidal Numerical Integration has been used to derive TSI within each time window which is defined by a series of 'Start time' and 'End time' (i.e. width of the time window). The comparison results regarding the coil EMF signals (single pipe casing - 5-1/2" pipe; double pipe casings - 5-1/2" pipe and 9-5/8" pipe) and TSIs of double pipe casings are shown in Fig. 4 and Fig. 5, respectively.

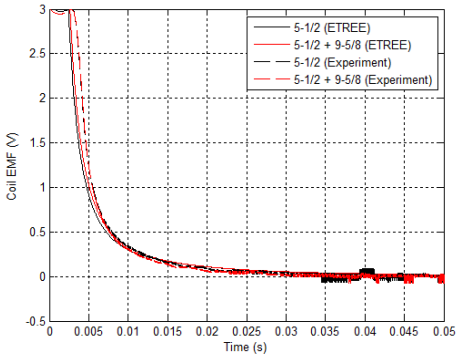

Fig. 4. Comparison of coil EMF signals for single pipe casing and double pipe casings beween ETREE and experiments

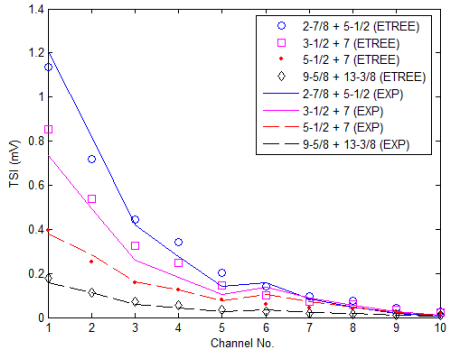

Fig. 5. Comparison of TSIs for double pipe casings beween ETREE and experiments

It can be seen from Fig. 4 and 5 that the coil EMF signals derived from ETREE have good agreement with experimental results with only minor discrepancies. The comparison results indicate that ETREE is valid and applicable to predict PEC signals for detection and evaluation of corrosion in multilayered pipe casings.

Results from the Inverse model.

From the measured signals as well as extracted TSIs, the wall-thinning occurring in inner and outer pipe casings could be inversely derived by using inverse models. Prior to the establishment of an inverse model, the correlations of TSIs with variations in thicknesses of inner and outer pipe casings and the sensitivities of individual TSIs to the wall-thinning are analyzed via a series of simulations conducted using ETREE. Suppose that double pipe casings are inspected with the inner and outer pipe casings as a typical oilfield pipe size combination. Two cases are investigated: (1) the thickness of the inner pipe casing decreases from 0% to -90% of the base thickness, whilst the thickness of the outer pipe casing doesn't vary; and (2) the thickness of the outer pipe casing decreases from 0% to -90% of the base thickness, whilst the thickness of the inner pipe casing keeps invariant. The correlations of TSIs with the wall-thinning for the two cases are presented in Fig. 6.

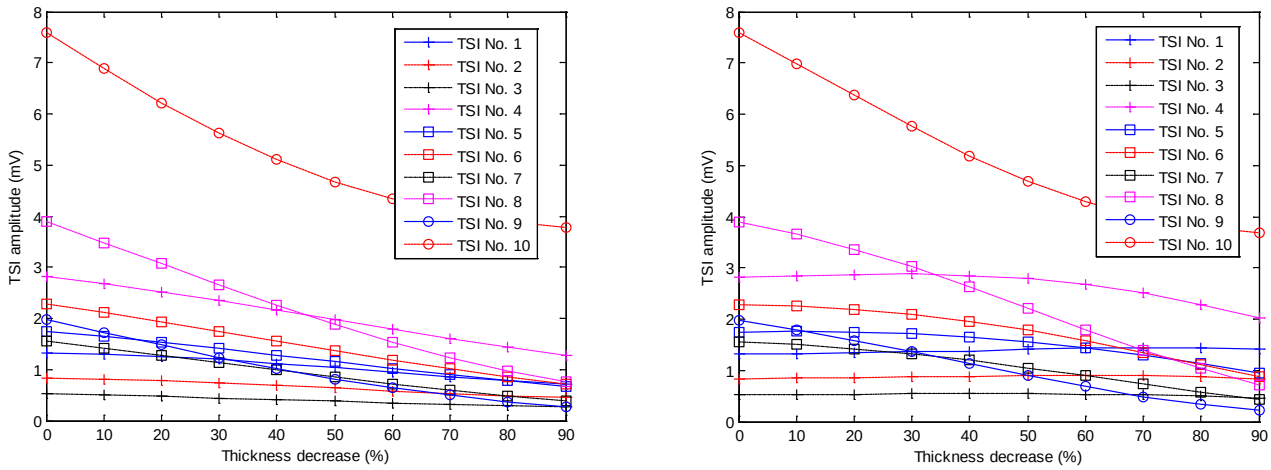

(a) **(b)**

Fig. 6. Correlations between TSIs of different channels and the wall-thinning of (a) inner pipe casing and (b) outer pipe casing

It can be found from Fig. 6(a) that the TSI amplitude decreases when the wall-thinning of the inner pipe casing is increased. As can be seen in Fig. 6(b), the amplitudes of TSIs No. 6 to 10 reduce with increasing wall-thinning of the outer pipe casing, which represents a similar trend of the correlation to that shown in Fig. 6(a). In contrast, the correlations of TSIs No 1 to 5 with the wall-thinning of the outer pipe casing show the opposite trend. This indicates the insensitivities of early-time TSIs (i.e. TSIs No. 1 to 5) to the decrease in thickness of the outer pipe casing.

Further analysis focusing on the sensitivities of TSIs to the wall-thinning of inner and outer pipe casings is carried out by taking first-order derivatives of TSI amplitudes against the wall-thinning. The computation of the first-order derivative gives the ratio of variation in each TSI to the thickness change of the pipe casing. The results are presented in Fig. 7.

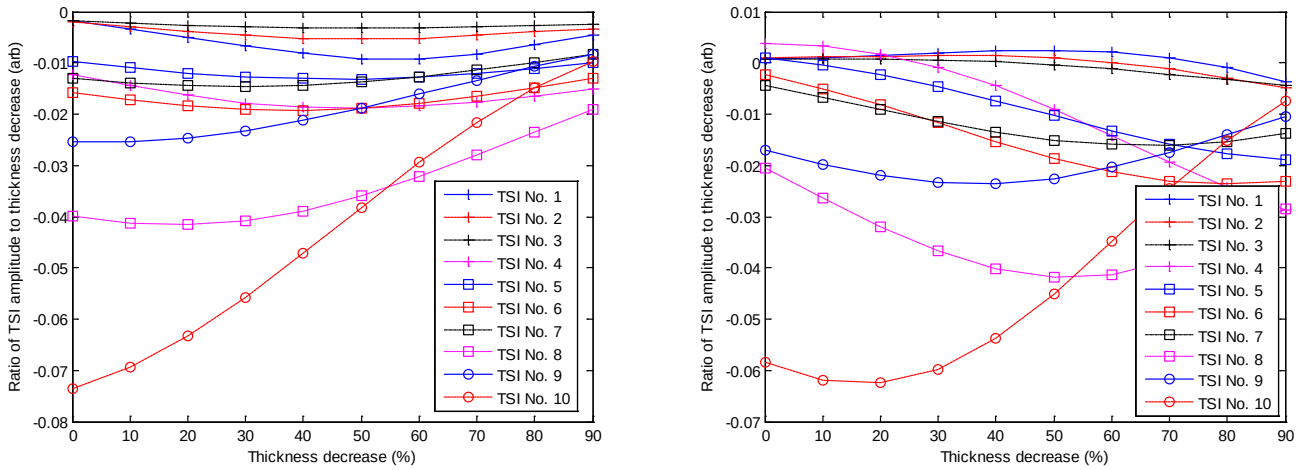

(a) **(b)**

Fig. 7. Sensitivities of TSIs of different channels to the wall-thinning of (a) inner pipe casing and (b) outer pipe casing

It is noteworthy that the negative values in Fig. 7 indicate the inverse proportion of the TSI amplitude to the wall-thinning. It can be seen in Fig. 7(a) that the TSI No. 10 has relatively higher sensitivity to the wall-thinning of the inner pipe casing. However, the ratio of TSI amplitude varies with the wall-thinning, which implies that the correlation between TSI No. 10 and the wall-thinning of the inner pipe casing is highly non-linear. This causes difficulty in identifying the wall-thinning in an inverse process. Therefore, TSI No. 4, which has relatively better linearity of the correlation, should be chosen for characterization of the wall-thinning of the inner pipe casing in this example pipe combination. The positive values for TSIs No. 1 to 5 can be found in Fig. 7(b), which indicates that TSIs No. 1 to 5 are insensitive to the wall-thinning of the outer pipe casing. In consideration of the linearity and absolute magnitude of TSI ratio, in this example a TSI No. 9 should be selected for classification of the wall-thinning of the outer pipe casing.

Following the sensitivity analysis of TSI, the inverse model is established, which is shown in Fig. 8. It is noted that at the first stage of the inversion, the nominal values of parameters of the standard pipe casings under evaluation need to be input in the forward model to work out the coil EMF signals and corresponding TSIs subject to different wall-thinning cases (inner or outer pipe casing, percentage of thickness decrease). In order to employ the TSIs of all channels for evaluation of an unknown wall-thinning, the weighting coefficient for each TSI is derived from the first-stage results. With respect to individual wall-thinning scenarios (wall-thinning in inner and outer pipe casings), the weighting coefficients (namely $[\alpha_n]$) of TSIs in different channels are calculated via the matrix-inversion algorithm, which is exhibited in mathematical manner as:

$$\begin{bmatrix} TSI_1 \\ TSI_2 \\ TSI_3 \\ \dots \\ TSI_{10} \end{bmatrix} \times \begin{bmatrix} \alpha_1 \\ \alpha_2 \\ \alpha_3 \\ \dots \\ \alpha_{10} \end{bmatrix} = \begin{bmatrix} H_1 \\ H_2 \\ H_3 \\ \dots \\ H_{10} \end{bmatrix} \Rightarrow \begin{bmatrix} \alpha_1 \\ \alpha_2 \\ \alpha_3 \\ \dots \\ \alpha_{10} \end{bmatrix} = \begin{bmatrix} H_1 \\ H_2 \\ H_3 \\ \dots \\ H_{10} \end{bmatrix} \times \begin{bmatrix} TSI_1 \\ TSI_2 \\ TSI_3 \\ \dots \\ TSI_{10} \end{bmatrix}^{-1} \tag{6}$$

where, $[TSI_n]$ and $[H_n]$ denote the matrices of the computed TSIs of all channels and percentage of pipe-casing thickness decrease, respectively. Thus, the estimated percentage (namely H_{est}) of pipe-casing thickness decrease of an unknown wall-thinning can be obtained via:

$$H_{est} = f\left(TSIs\right) = \sum_{n=1}^{10} \alpha_n TSI_n^{'} \tag{7}$$

where, TSI_n' denotes the measured TSIs of all the channels for the unknown wall-thinning. Based on the simulation results presented in Fig. 6, the weighting coefficients of TSIs for the two scenarios are computed by using Eq. (6) and listed in Table 3.

It is noteworthy that in order to enhance the accuracy of the inversion, iteration process has been adopted. After H_{est} is obtained during the first iteration, it is input in the forward solver to compute the corresponding TSIs. By using Eq. (7), a new H_{est}' is derived. The residual between H_{est} and H_{est}' is computed. The iteration terminates when the residual is less than the tolerance ε, otherwise H_{est} is updated using $H_{est}= H_{est}'+\varepsilon$ and the iteration continues until the termination condition is met.

Table 3. Weighting coefficients of TSIs for typical double pipe casings

	α_1	α_2	α_3	α_4	α_5	α_6	α_7	α_8	α_9	α_{10}
Wall-thinning in inner pipe casing	0.0145	0.009	0.0054	0.0276	0.0157	0.0182	0.011	0.0241	0.0103	0.0701
Wall-thinning in outer pipe casing	0.0223	0.0139	0.0081	0.0395	0.0211	0.023	0.0131	0.0268	0.0106	0.0696

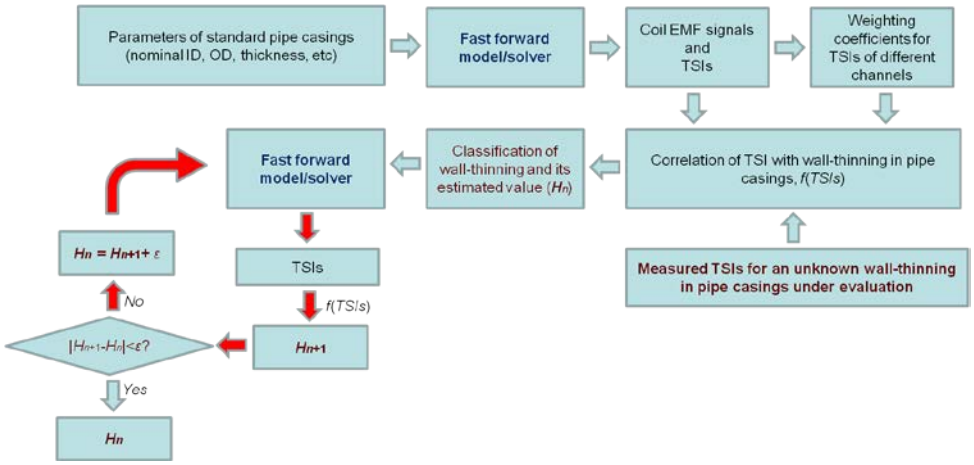

Fig. 8. Schematic illustration of the inverse model

Conclusions

This paper introduces the theoretical basis of using Pulsed Eddy Current (PEC) for a slim-hole logging tool that is sensitive to defects and corrosion in multiple well tubular, including both tubing and casing. The work outlines the methodology for data processing of the PEC signals and the associated interpretation principles. Other work [14, 15] demonstrates the field application of this PEC technology.

References:

[1] J. W. Wilson and G. Y. Tian, "3D magnetic field sensing for magnetic flux leakage defect characterisation", Insight, Vol. 48, No. 6, 2006, pp. 357-359.
[2] Y. Li, G. Y. Tian and S. Ward, "Numerical simulation on Magnetic Flux Leakage Evaluation at high speed", NDT&E International, Vol. 39, No. 5, 2006, pp. 367-373.
[3] J. B. Nestleroth, "Implementing current in-line inspection technologies on crawler systems", Technology Status Report, http://www.netl.doe.gov/, April 2004, pp. 1-14.
[4] G. Y. Tian, A. Sophian, D. Taylor and J. R. Rudlin, "Pulsed eddy current system for dynamic inspection of defects", Insight, Vol. 46, No. 5, May 2004, pp. 256-259.
[5] Sophian, G. Y. Tian, D. Taylor and J. Rudlin, "Design of a pulsed eddy current sensor for detection of defects in aircraft lap-joints", Sensors and Actuators A: Physical, Vol. 101, No. 1-2, September 2002, pp. 92-98.
[6] Y. Li, Z. M. Chen, Y. Mao and Y. Qi, "Quantitative evaluation of thermal barrier coating based on eddy current technique", NDT&E International, Vol. 50, 2012, pp. 29-35.
[7] Y. Li, G. Y. Tian and S. Ward, "Finite Element Analysis of Remote Field Eddy Current Inspection of Metallic Coated Pipeline", Proceedings of the 12th Chinese Automation & Computing Society Conference in the UK, Loughborough, England, 16 September 2006, pp. 23-27.
[8] A. Sophian, G. Y. Tian, D. Taylor and J. Rudlin, "Design of a pulsed eddy current sensor for detection of defects in aircraft lap-joints", Sensors and Actuators A: Physical, Vol. 101, No. 1-2, September 2002, pp. 92-98.
[9] S. J. Xie, T. Takagi, T. Uchimoto, Z. M. Chen and L. Wang, "An Inversion Scheme for Sizing of Wall Thinning Defect from Pulsed ECT Signals", Journal Studies in Applied Electromagnetics and Mechanics, Vol.14, 2011, pp.293-294.
[10] Y. Li, G. Y. Tian and A. Simm, "Fast analytical modelling for pulsed eddy current evaluation", NDT&E International, Vol. 41, No. 6, 2008, pp. 477-483.
[11] Y. Li, T. Theodoulidis and G. Y. Tian, "Magnetic field-based eddy-current modeling for multilayered specimens", IEEE Transactions on Magnetics, Vol. 43, No. 11, November 2007, pp. 4010-4015.
[12] Y. Li, "Theoretical and Experimental investigation of Electromagnetic NDE for defect characterisation", Newcastle University, 2008.
[13] T. Theodoulidis, E. Kriezis, "Eddy current canonical problems (with applications to nondestructive evaluation)", TechScience Press, 2006.
[14] R. Ahmed R, M Rana, A. Pamungkas, I Sajjad, "Effective and Eco-Efficient Pipe Inspection in Heavy Mud Environment Using Induced Electro-Magnetic Measurement (EMDS)" SPE 156207
[15] J. Garcia, K. Yateem, N. Sethi, N. Guergueb, "Successful Application of a New Electromagnetic Corrosion Tool for Well Integrity Evaluation in old wells completed with reduced diameter tubular", IPTC-16997 2013